

Shockwaves in Supernovae: New Implications on the Diffuse Supernova Neutrino Background

Sébastien Galais,^{*} James Kneller,[†] Cristina Volpe,[‡] and Jérôme Gava[§]

*Institut de Physique Nucléaire, F-91406 Orsay cedex,
CNRS/IN2P3 and University of Paris-XI, France*

(Dated: June 3, 2018)

We investigate shock wave effects upon the diffuse supernova neutrino background using dynamic profiles taken from hydrodynamical simulations and calculating the neutrino evolution in three flavors with the S-matrix formalism. We show that the shock wave impact is significant and introduces modifications of the relic fluxes by about 20% and of the associated event rates at the level of 10 – 20%. Such an effect is important since it is of the same order as the rate variation introduced when different oscillation scenarios (i.e. hierarchy or θ_{13}) are considered. In addition, due to the shock wave, the rates become less sensitive to collective effects, in the inverted hierarchy and when $\sin^2 2\theta_{13}$ is between the Chooz limit and 10^{-5} . We propose a simplified model to account for shock wave effects in future predictions.

PACS numbers: 14.60.Pq, 97.60.Bw

Keywords:

I. INTRODUCTION

Our understanding of neutrino propagation through supernovae has been revolutionized by the demonstration that non-linear effects and the dynamism of the density profile can have significant impact. The neutrino density close to the last scattering surface at the neutrinosphere is so large that it generates significant off-diagonal contributions to the effective potential describing neutrino evolution in matter [1]. This neutrino-neutrino interaction gives rise to collective behavior regimes known as synchronization, bipolar oscillations and spectral splits [2, 3, 4, 5, 6, 7]. At the same time, the evolution of the supernova density profile as the shock wave races through the mantle, has been found to change the adiabaticity of the high-density (H) resonance [8, 9, 10, 11, 12, 13, 14, 15, 16, 17] engendering instances of multiple H resonances [15, 17, 18] which have been shown to lead to phase effects. Thus, the neutrino evolution and the emerging spectra involve an interplay between these two effects that might lead to observable consequences for any future Galactic supernova neutrino signal [19].

Very complementary information to the measurement of neutrinos from a single core-collapse supernova come from the observation of the diffuse supernova neutrino background (DSNB). Its detection would represent a crucial step forward in our understanding of neutrino properties, of the star formation rate and of the supernova dynamics. The current upper limits are $6.8 \times 10^3 \nu_e \text{ cm}^{-2}\text{s}^{-1}$ with $25 \text{ MeV} < E_{\nu_e} < 50 \text{ MeV}$ (90 % C.L.)

from LSD [29] and $1.08 \bar{\nu}_e \text{ cm}^{-2}\text{s}^{-1}$ with $E_{\bar{\nu}_e} > 19.3 \text{ MeV}$ from Super-Kamiokande [30]. Next-generation neutrino observatories [31], currently under study, should possess the discovery potential to observe the DSNB (see e.g. [26, 27, 28] and references therein). To be able to disentangle the information encoded by the explosion mechanism, neutrino properties and the star formation rate it is important to observe both the $\bar{\nu}_e$ via the scattering on protons and ν_e through neutrino-nucleus interactions e.g. on ^{40}Ar [32] or ^{12}C and ^{16}O [33]. Another strategy to observe the DSNB is to exploit upgraded technologies, such as the addition of Gadolinium to water Cherenkov detectors [34], to reach the sensitivity for a discovery with the running Super-Kamiokande detector. Finally, relic supernova neutrinos could be searched for through a geological measurement [20] of the amount of Technetium-97 produced in Molybdenum-98 ore [38], if high-precision solar data and precise neutrino-nucleus cross sections become available [39].

Simultaneously, progress is being made with regard to the accuracy of the predictions and many calculations have been performed to predict the relic neutrino fluxes and rates [20, 21, 22, 23, 24, 25, 26, 27, 28]. The star formation rate has now been constrained by combining various astrophysical observations [35] even at high redshifts [36], though the local value at $z = 0$ retains a factor of 2 uncertainty. The calculations of the neutrino propagation in the supernova now include the effects induced by the resonant flavor conversion in matter and recently also the flux modifications induced by the neutrino-neutrino interaction [37].

Our aim in this paper is to show that the shock wave effects upon the DSNB are considerable. To this end we follow numerically the neutrino evolution (with and without neutrino self interactions) in a core-collapse supernova using dynamical density profiles from hydrodynamical simulations. We analyze the impact of shock waves both on the relic (anti)neutrino fluxes and on the

^{*}Electronic address: galais@ipno.in2p3.fr

[†]Electronic address: kneller@ipno.in2p3.fr

[‡]Electronic address: volpe@ipno.in2p3.fr

[§]Electronic address: gava@ipno.in2p3.fr

associated number of events in an observatory on Earth based on different technologies. Furthermore, we show that the shockwaves reduce the sensitivity of the DSNB to collective effects when θ_{13} is above $\sin^2 2\theta_{13} > 10^{-5}$. A simplified model allows us to quantitatively account for the shockwave impact, which we use to test the robustness of our results.

The paper is structured as follows. Section II presents the formalism. The results on the relic neutrino fluxes and associated rates are described in Section III. Our simplified model as well as the discussion on the robustness of the results, also in presence of turbulence, are included as well. Section IV is a conclusion.

II. THEORETICAL FRAMEWORK

The DSNB flux at Earth, as a function of neutrino energy E_ν , is calculated as

$$F_\alpha(E_\nu) = \int dz \left| \frac{dt}{dz} \right| (1+z) R_{SN}(z) \frac{dN_\alpha(E'_\nu)}{dE'_\nu} \quad (1)$$

where z is the redshift, $E'_\nu = (1+z)E_\nu$, R_{SN} is the core-collapse supernova rate per unit comoving volume and dN_α/dE_ν is the differential spectra emitted by each supernova. The most involved component of the calculations is the determination of the neutrino spectra at the supernova, dN_α/dE_ν . Our calculation proceeds in two steps, the first to account for the collective effects and the second the dynamic MSW.

The neutrino wavefunction $\psi(\mathbf{p}, \mathbf{r})$ evolves according to the Schroedinger-like equation

$$i \frac{d\psi}{dt} = [H_0(E_\nu) + H_m(\mathbf{r}) + H_{\nu\nu}(\mathbf{p}, \mathbf{r})] \psi \quad (2)$$

where $H_0(E_\nu)$ is the Hamiltonian describing the vacuum oscillations. In the mass basis H_0 is diagonal and is related to the flavor basis through $H_0^{(f)} = U H_0^{(m)} U^\dagger$, where U is the unitary Maki-Nakagawa-Sakata-Pontecorvo matrix parameterized by three mixing angles - θ_{12} , θ_{13} , θ_{23} - and six phases though only one, the CP phase, δ , is relevant for oscillations. The second term in the Hamiltonian is the neutrino interaction with matter and is diagonal in the flavor basis i.e. $H_m^{(f)}(\mathbf{r}) = \text{diag}(V_e(\mathbf{r}), V_\mu(\mathbf{r}), V_\tau(\mathbf{r}))$. Only the differences between the potentials are relevant. The difference $V_e - V_\mu$ is the well known $V_e - V_\mu = \sqrt{2} G_F N_e(\mathbf{r})$ with $N_e(\mathbf{r})$ the electron density. At tree level $V_\mu = V_\tau$ in normal matter because there are no charged leptons present other than electrons; the difference ($V_\tau - V_\mu$) is due to loop corrections and within the standard model its ratio with respect to V_e is very small, $\mathcal{O}(10^{-5})$ [40], however supersymmetric corrections can increase it to the level of $\mathcal{O}(10^{-3})$ [41]. The final contribution to the Hamiltonian is the neutrino self-interaction term, calculated as in [42], using the single-angle approximation. It has been shown that this approximation

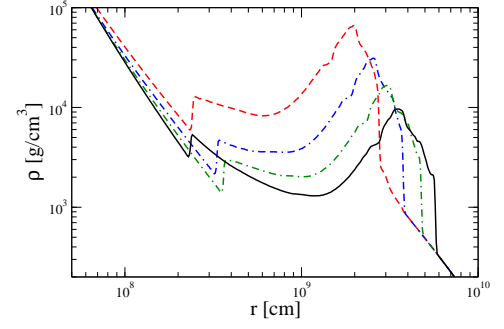


FIG. 1: Density profiles with front and reverse shocks as a function of distance in the star. The curves correspond to 1.5 (dashed), 2 (double-dot-dashed), 2.5 (dot-dashed) and 3 seconds (full line) post-bounce.

reproduces both qualitatively and quantitatively the results of multi-angle calculations [3]. Using this approximation $H_{\nu\nu}(\mathbf{p})$ becomes

$$H_{\nu\nu} = \frac{\sqrt{2} G_F}{2\pi R_\nu^2} D(r/R_\nu) \sum_\alpha \int [\rho_{\nu_\alpha}(q') L_{\nu_\alpha}(q') - \rho_{\bar{\nu}_\alpha}^*(q') L_{\bar{\nu}_\alpha}(q')] dq' \quad (3)$$

with the geometrical factor

$$D(r/R_\nu) = \frac{1}{2} \left[1 - \sqrt{1 - \left(\frac{R_\nu}{r} \right)^2} \right]^2 \quad (4)$$

where the radius of the neutrino sphere is $R_\nu = 10$ km, and $L_{\nu_\alpha}(q')$ are the neutrino fluxes at the neutrino-sphere. The sum in Eq.(3) is over the initial neutrino flavor at the neutrino-sphere while the integral is performed over the different neutrino energies. Both neutrinos and anti-neutrinos contribute to the neutrino-neutrino interaction term. Once the calculations of this step are completed we construct the two evolution operators $S(r_\star, 0)$ and $\bar{S}(r_\star, 0)$ ($r_\star = 1000$ km) at each neutrino energy.

The second step is to determine the (anti)neutrino evolution from r_\star through to the supernova surface R . Here the shock wave effects will appear. We take supernova matter density profiles from a one-dimensional, hydrodynamical simulation described in [17] (Figure 1). The explosion of an ‘initial’, standing accretion shock profile is triggered by the injection of 3.36×10^{51} erg of energy into a region beyond a 100 km gain radius, in a fashion similar to neutrino heating. The heating creates a wind and falls off exponentially with time. The profiles contain forward and reverse shocks [12, 17, 43], created by the wind, with a large bubble/cavity in-between. The neutrino evolution through the density profiles again follows equation (2) but beyond $r \sim 1000$ km the self interaction effects are negligible. At the end of this step we again construct the evolution operators $S(R, r_\star)$ and $\bar{S}(R, r_\star)$.

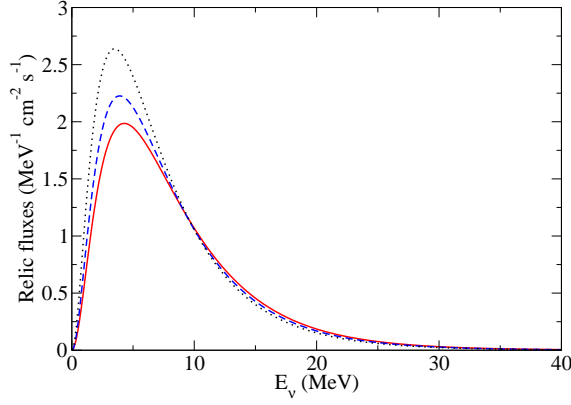


FIG. 2: Relic ν_e flux on Earth, as a function of neutrino energy, in the case of normal hierarchy, with the neutrino-neutrino interaction and shock wave effects and case L from the numerical calculations (dashed line, see text). The other two curves are derived from the analytic formulae [17, 54] for either case S (dotted) or case L (solid) and include the neutrino-neutrino interaction but no shock wave. Note that in the case S the analytical and numerical results are equal.

As in [19] we suture together the results of the two steps by multiplying in time order the evolution operators i.e. $S(R, 0) = S(R, r_*)S(r_*, 0)$ and $\bar{S}(R, 0) = \bar{S}(R, r_*)\bar{S}(r_*, 0)$ rather than probabilities c.f. [17, 37, 50]. Any possible interference effects are thus captured. We then take into account decoherence due to the divergence of the wavepackets and, finally, calculate the ν_e and $\bar{\nu}_e$ survival probabilities $p(E_\nu, t)$ and $\bar{p}(E_\nu, t)$.

The results we present here are obtained with the following parameters. At the neutrino sphere radius we adopt Fermi-Dirac distributions for the spectra and make the assumption of energy equipartition among the flavors, $L_\alpha = 10^{52}$ erg/s each at $t = 0$ s, with $L(t) \propto \exp(-t/\tau)$, with a cooling time of $\tau = 3.5$ s. The average neutrino energies follow a hierarchy i.e. $\langle E_{\nu_e} \rangle < \langle E_{\bar{\nu}_e} \rangle < \langle E_{\nu_x} \rangle$ with values of 12, 15 and 18 MeV respectively. We take $\delta m_{12}^2 = 8 \times 10^{-5} \text{eV}^2$, $|\delta m_{23}^2| = 3 \times 10^{-3} \text{eV}^2$, $\sin^2 2\theta_{12} = 0.83$ and $\sin^2 2\theta_{23} = 1$ [45]. The CP phase δ is here set to zero. For a discussion of the conditions under which it can modify the neutrino fluxes and its possible effects see [42, 46, 47]. We shall explore both the normal and inverted hierarchies and consider two cases for the unknown angle θ_{13} : a large value $\sin^2 2\theta_{13} = 4 \times 10^{-4}$ (case L) which lies above the $\sin^2 2\theta_{13} > 10^{-5}$ threshold [48], and a much smaller value, $\sin^2 2\theta_{13} = 4 \times 10^{-8}$ (case S), below the threshold. Note that the results corresponding to θ_{13} large are valid for the range $\sin^2 2\theta_{13} \in [0.19, 10^{-5}]$.

Concerning the other terms that appear in Eq.(2), we adopt a flat Universe so that

$$dz/dt = -H_0(1+z)\sqrt{\Omega_m(1+z)^3 + \Omega_\Lambda} \quad (5)$$

and use the concordance Λ CDM model parameters $\Omega_\Lambda = 0.7$ and $\Omega_m = 0.3$. To calculate R_{SN} , we take the star

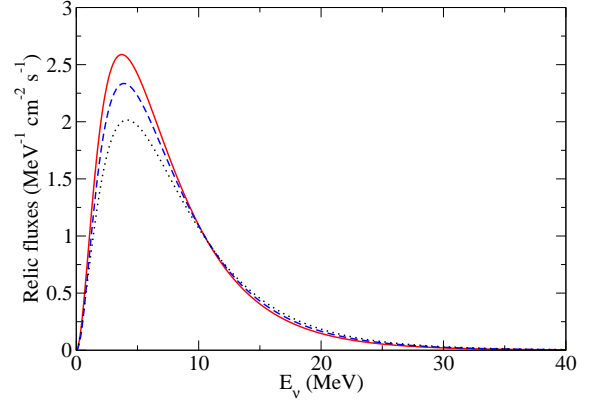


FIG. 3: Same as Fig.2 but for the relic $\bar{\nu}_e$ flux on Earth in the case of inverted hierarchy.

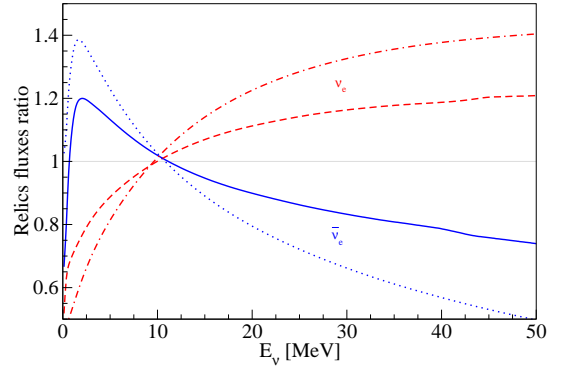


FIG. 4: Relic electron (anti-)neutrino flux ratios on Earth, with $\sin^2 2\theta_{13} = 4 \times 10^{-4}$ (case L) over $\sin^2 2\theta_{13} = 4 \times 10^{-8}$ (case S), as a function of neutrino energy. The numerical results concerning the relic fluxes are shown for $\bar{\nu}_e$ in inverted hierarchy (solid) and ν_e in normal hierarchy (dashed) include shock wave effects and the $\nu\nu$ interaction. Note that the results corresponding to the larger value of θ_{13} are valid for the whole range $\sin^2 2\theta_{13} \in [0.19, 10^{-5}]$. For comparison, the ratios for $\bar{\nu}_e$ (dotted) and ν_e (dot-dashed) as computed from the analytical formulae [17, 54] are also given. In these formulae the $\nu\nu$ interaction is included but there are no shock wave effects.

formation rate (R_{SF}) from [36], use the relation

$$R_{SN}(z) = R_{SF}(z) \frac{\int_{8M_\odot}^{125M_\odot} \varphi(m) dm}{\int_{0.1M_\odot}^{125M_\odot} \varphi(m) m dm}, \quad (6)$$

and adopt the initial mass function from [44]

$$\varphi(m) \propto \begin{cases} m^{-1.50} & (0.1M_\odot < m < 0.5M_\odot) \\ m^{-2.25} & (m > 0.5M_\odot) \end{cases}. \quad (7)$$

III. RESULTS

A. Results on the DSNB fluxes and rates

Our goal is to show that the shock wave effects upon the DSNB fluxes and on the expected event rates in water Cerenkov, scintillator and liquid argon detectors are significant. We then elucidate that the effects can be rather well accounted for by considering four main contributions: the pre-shock, the shock, the phase effects and the post-shock. This quantitative analysis allows us to propose a schematic model to account for shock wave effects in future predictions.

The numerical results for the relic fluxes and case L - including the $\nu\nu$ interaction - are shown for ν_e in a normal hierarchy in Figure 2 and for $\bar{\nu}_e$ in the inverted hierarchy in Figure 3. We also show the relic fluxes computed from analytical formulas for comparison where we set: $P_H = 0$ for case L and $P_H = 1$ for case S for all times [17, 37]. These analytical formulas do not include any shock wave effects (while they include the effect of the neutrino-neutrino interaction). Figure 4 presents the ratios of the relic (anti)neutrino fluxes for case L value to the case S value so that the high energy tail is more visible. Note that this ratio is directly sensitive to the shock because the shock affects the neutrino propagation only for case L, while for case S the relic flux is identical to that obtained with the analytical formulas. Figures 2-4 show the analytical results including $\nu\nu$ interaction but no shock wave are at variance with the numerical results which include shock effects : the difference between the analytical fluxes computed with no shocks and numerical ones for the two values of θ_{13} is reduced roughly by half.

This result is at variance with [49] where it was found that shock wave effects were negligible. Such a difference might be due to the fact that, as stated in [8, 11, 17], the shocks in hydrodynamical profiles are ‘softened’ due to numerical artifacts and are not as steep as they should be. Since the adiabaticity is inversely proportional to the density derivative, a softened shock is more adiabatic than a non-softened shock. This is why the choice for a ‘large’ θ_{13} , as in Ref.[49], seems to give an adiabatic result (lower panel of figure 1 in [49]). To compensate for the softness of the shocks in hydro-profiles one must either steepen the shock feature by hand, e.g. as in [8, 12], or use a value of θ_{13} (case L) as close as possible to the threshold $\sin^2 2\theta_{13} > 10^{-5}$ but without making the adiabaticity of the progenitor too small, as in e.g. [17].

After computing the relic fluxes we can then compute the DSNB event rates in a detector with both our numerical results and using the fluxes computed using the analytic formulae. We shall consider three types of detector: water Cerenkov, scintillator and liquid argon. While in the former the main detection channel is $\bar{\nu}_e + p$, in the latter ν_e are observed through ^{40}Ar scattering. The computed event rates are shown in I and II.

Table I presents a comparison between the event rates for case L obtained with the analytical formulas – that

$\bar{\nu}_e$ events			
case	Window	Numerical	Analytical
IH	19.3-30 MeV	0.070	0.059
IH	9.3-25 MeV	0.190	0.176
NH	19.3-30 MeV	0.059	0.059
NH	9.3-25 MeV	0.176	0.176

ν_e events			
case	Window	Numerical	Analytical
NH	17.5-41.5 MeV	0.059	0.067
NH	4.5-41.5 MeV	0.095	0.104
IH	17.5-41.5 MeV	0.053	0.068
IH	4.5-41.5 MeV	0.089	0.105

TABLE I: Comparison between numerical (with shock wave) and analytical (without shock wave) DSNB event rates (/kton/year), for the case of large θ_{13} (L). The results correspond to $\bar{\nu}_e + p$ and $\nu_e + ^{40}\text{Ar}$ scattering, in different experimental windows, relevant for water Cerenkov, scintillator and argon detectors. The $\nu\nu$ interaction is included in all cases.

Inverted Hierarchy: with $\nu\nu$ (without $\nu\nu$)			
N_{events}	Window	L	S
$\bar{\nu}_e$	19.3-30 MeV	0.070 (0.070)	0.080 (0.059)
$\bar{\nu}_e$	9.3-25 MeV	0.190 (0.189)	0.202 (0.176)

Normal Hierarchy : with/without $\nu\nu$		
N_{events}	Window	L or S
$\bar{\nu}_e$	19.3-30 MeV	0.059
$\bar{\nu}_e$	9.3-25 MeV	0.176

Normal Hierarchy : with/without $\nu\nu$			
N_{events}	Window	L	S
ν_e	17.5-41.5 MeV	0.059	0.052
ν_e	4.5-41.5 MeV	0.095	0.086

Inverted Hierarchy: with $\nu\nu$ (without $\nu\nu$)		
N_{events}	Window	L or S
ν_e	17.5-41.5 MeV	0.053 (0.052)
ν_e	4.5-41.5 MeV	0.089 (0.086)

TABLE II: DSNB event rates/kton/year for $\bar{\nu}_e + p$ and $\nu_e + ^{40}\text{Ar}$ scattering, from our numerical calculations, relevant for water Cerenkov, scintillator and argon detectors. The large θ_{13} (L) and small (S) cases are the same as in Figure 4. The calculations include shock waves effects, with/without the neutrino-neutrino ($\nu\nu$) interaction.

only take into account a single MSW resonance – with the numerical calculations which include the shock effects. Both calculations include the neutrino-neutrino interaction. One can see that, indeed, when one includes the shock wave the rates are modified by 10 – 20% relative to the analytic formulae showing that the shock wave

impact the rates significantly. This is true both in the inverted hierarchy for $\bar{\nu}_e$ and in the normal hierarchy for ν_e . On the other hand, if θ_{13} is small, analytical and numerical results are equal in the inverted hierarchy and $\bar{\nu}_e$. However, for ν_e and normal hierarchy a discrepancy of about 20 % between the two calculations appear. We have found that such a difference is a combined effect of the $V_{\mu\tau}$ refractive index with the $\nu\nu$ interaction. Let us now discuss the rate sensitivity to different oscillation scenarios.

Table II presents the DSNB rates obtained from the numerical calculations only for normal/inverted hierarchy and large/small θ_{13} . The DSNB rates change between 7 to 15 % when one goes from the L to the S case, both in the neutrino (normal hierarchy) and in the anti-neutrino (inverted hierarchy) channels. Such a variation is of the same order as the shock wave effects previously discussed. As already suggested by Figs. 2-4, the rate variation from L to S cases given by the approximate analytical formulas is reduced by half compared to the numerical calculations showing again that including the shock wave is important. Finally the numerical results for $\bar{\nu}_e$ are the same for normal hierarchy if θ_{13} is L or S.

From Table II the effect of the $\nu\nu$ interaction in presence of the shock wave can also be seen. If we focus upon $\bar{\nu}_e$ and case L we observe a most surprising result: when shock wave effects are included the $\bar{\nu}_e$ DSNB rates lose their sensitivity to the collective effects. On the other hand, the event rates for ν_e in inverted hierarchy increase slightly because of the spectral split that is induced when the $\nu\nu$ interaction is included. For the $\bar{\nu}_e$ DSNB event and case S, we see that the $\nu\nu$ interaction alone leads to an increase of around 10-30%.

Before going on to explain why the sensitivity to the $\nu\nu$ interaction is lost, in presence of the shock wave, we can use these calculations to predict, on average, 343, 91 and 62 events over 10 years in a detector like MEMPHYS (440 kton), LENA (50 kton) or GLACIER (100 kton) respectively.

B. A simplified model to account for shock wave effects

To gather further insight on the robustness of our results - and of the loss of sensitivity to the collective effects - we have built up a simplified model for our numerical calculations. At any given energy the time-integrated $\bar{\nu}_e$ spectra are

$$\frac{dN_{\bar{e}}}{dE} = \int_0^\infty dt (\bar{p}\Phi_{\bar{e}} + (1 - \bar{p})\Phi_{\bar{x}}). \quad (8)$$

where $\Phi_\alpha(E, t)$ are the spectra at the neutrinosphere. The time dependence of $\bar{p}(E, t)$ can be summarized as follows. At around $t \sim 2$ s into the supernova the shock wave reaches the H resonance region. If the value of θ_{13} is large then the adiabatic evolution prior to the shock

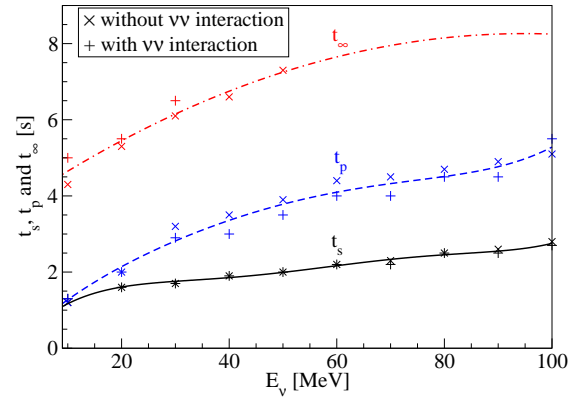


FIG. 5: Numerical results on the three times characterizing the neutrino evolution, with shock waves, in the supernova mantle : the shock t_s , the phase-effects t_p and the post-shock t_∞ . The corresponding analytical fits are also shown.

becomes non-adiabatic when the shock arrives. Non-adiabatic propagation persists for some time and then switches to a period where the survival probability oscillates rapidly due to phase effects generated by multiple H resonances. These eventually cease whereupon neutrino propagation enters a post-shock regime that may be adiabatic or semi-adiabatic depending upon θ_{13} and the post-shock profile. The shock affects lower neutrino energies before the higher and the duration of the non-adiabatic period grows with neutrino energy. This picture allows us to approximate the evolution of $\bar{p}(E, t)$ as a sequence of phases: a) the pre-shock interval up to $t_s(E)$, b) the shock interval from $t_s(E)$ to $t_p(E)$ c) the phase-effect interval from $t_p(E)$ to $t_\infty(E)$ d) the post-shock period from $t_\infty(E)$ onwards. In this way we divide the integral in Eq.(8) into four. The transition times taken from the numerical results as a function of neutrino energy are shown in Figure 5. The curves have been fitted with polynomials given by

$$t_{s,p}(E) = \sum_{i=0}^5 a_i \cdot E^i \quad (9)$$

$$t_\infty(E) = 3.75 + 9.5 \times 10^{-2} E - 5 \times 10^{-4} E^2 \quad (10)$$

with the coefficients given in Table III. We then ap-

	a_0	a_1	a_2
t_s	1.02×10^{-2}	1.72×10^{-1}	-6.88×10^{-3}
t_p	9.83×10^{-2}	1.39×10^{-1}	-2.47×10^{-3}

	a_3	a_4	a_5
t_s	1.4×10^{-4}	-1.2×10^{-6}	4.2×10^{-9}
t_p	4.0×10^{-5}	-4.4×10^{-7}	1.9×10^{-9}

TABLE III: Coefficients for the polynomial fit of Eq.(9).

proximate $\bar{p}(E, t)$ within each domain by using average \bar{p} value independent of E . These averages are shown in

Interval	$0 \rightarrow t_s$	$t_s \rightarrow t_p$	$t_p \rightarrow t_\infty$	$t_\infty \rightarrow \infty$
With $\nu\nu$	0.5436	0.0634	0.3092	0.2548
Without $\nu\nu$	0.1611	0.6356	0.3531	0.4835

TABLE IV: Average \bar{p} values from the numerical calculations, us

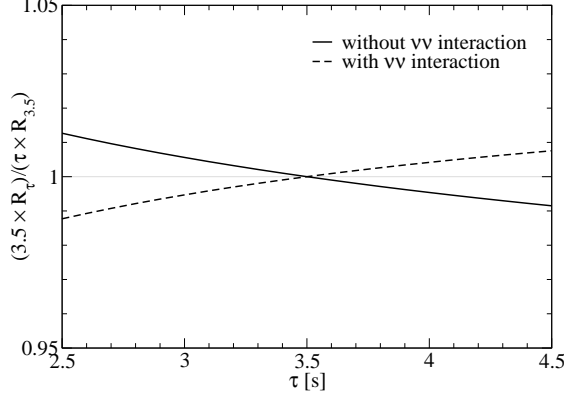


FIG. 6: The ratio of the $\bar{\nu}_e$ DNSB event rate with altered cooling time τ relative to the rate with $\tau = 3.5$ s for the inverted hierarchy and case L either with or without the neutrino self interaction effects. All parameters are as before including the neutrino luminosities so the additional τ factor accounts for the change in the overall neutrino luminosity.

Table IV. Using this schematic model we can quantitatively reproduce the rates obtained with or without the neutrino-neutrino interaction in the inverted hierarchy a)

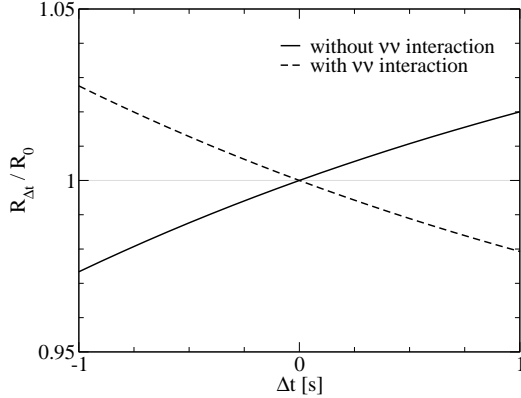


FIG. 7: The ratio of the $\bar{\nu}_e$ DNSB event rate when an offset Δt time is introduced relative to the rate with zero offset for the inverted hierarchy and case L either with or without the neutrino self interaction effects.

We can now use the simplified model just described to understand why, when the shock wave is present, we lose sensitivity to the collective effects. Indeed, when computing the DNSB relic fluxes for case L and a given hierarchy the effect of the shock leads to a time-integrated spectra that is composed of a mixture of pre-shock and post-

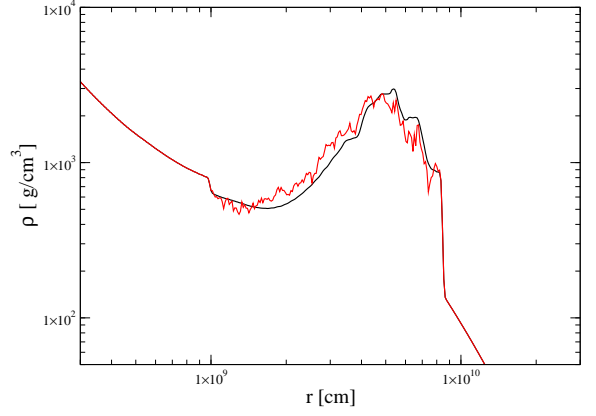


FIG. 8: One-dimensional density profile at 4.5 s with (dashed) and without noise (full line, see text).

shock fluxes. Due to the coincidence between the cooling time $\tau = 3.5$ s we selected and the arrival of the shock in the H resonance region, $t \sim 2$ s for the hydro model used, this mixture is almost exactly 50:50. It is because this composition is so close to equality that switching on or off the $\nu\nu$ collective effects has little impact for the $\bar{\nu}_e$ DNSB rates in case L and the inverse hierarchy. But if we change τ or alter the time at which the shock reaches the H resonances then we alter the mixture of pre- and post-shock fluxes that make the time-integrated spectra and thus might recover some sensitivity to the collective effects. To properly examine the sensitivity to the cooling time and/or shock dynamics we can use the simplified model.

C. Robustness of the results

Using the model described in the previous section we have investigated the sensitivity of our results to the neutrino mixing parameters, to the emission spectra and also to the shock dynamics. The ratio of the results with an altered τ relative to the fiducial rate at $\tau = 3.5$ s is shown in Figure 7. The additional τ factor accounts for the change in the integrated luminosity. For cooling times between 2.5 and 4.5 s the DNSB rates with and without neutrino-neutrino interaction, differ at most by 2–3%. We can also use the model to test the sensitivity to the profile dynamics. By introducing a temporal offset to all the times, so the new times are now $t_{s,p,\infty} + \Delta t$ we can alter the shock arrival time in the H resonance region. The ratio of the rates with non-zero Δt relative to the rate with no offset are shown in Figure 7. For reasonable values, $(\Delta t \pm 1\text{s})$, the difference does not exceed 4% from the rates listed in Table II. Thus we conclude that the loss of sensitivity to θ_{13} and to the collective effects is robust and is not an effect of the coincidence of our original choice of cooling time and the density profiles adopted.

Let us discuss the robustness of our results with respect to the possible presence of turbulence. The tran-

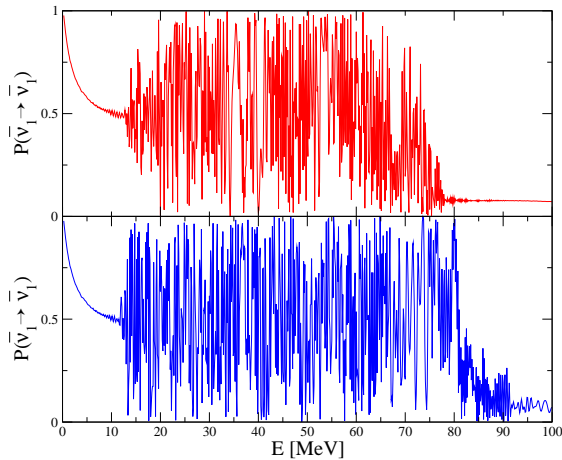


FIG. 9: Matter basis survival probability for $\bar{\nu}_1$ for inverted hierarchy and $\sin^2 2\theta_{13} = 4 \times 10^{-4}$ for the profiles of Figure 8 with no noise (upper) and with noise (lower figure).

sition from adiabatic to non-adiabatic propagation for case L is also a crucial factor in reducing the sensitivity to the collective effects. Any new effect or feature in the profiles that changes the size of the adiabatic to non-adiabatic transition would alter the composition of the time-integrated neutrino spectrum. The presence of turbulence may be such a feature. The restriction to spherical symmetry for the density profiles used in this paper means the profiles do not possess the small scale density fluctuations seen in two dimensional simulations [12, 17] generated by non-radial flow through aspherical shocks. But one also observes that the profiles in two dimensional simulations also possess common features with the one dimensional profiles: they both contain forward and reverse shocks with a cavity between them and any difference are in the details such as the ratio of shock heights or cavity depth. It is because of this similarity that we anticipate that adoption of a turbulent profile would not actually give very different results. Our reasoning is that at any given moment during the neutrino emission, the effect of strong turbulence is to create a range of neutrino energies with survival probabilities that are essentially randomly distributed from zero to unity [16, 51, 52, 53]. When averaged over an ensemble of fluctuation spectra strong turbulence tends to drive the neutrino oscillation probabilities to one-half. But, the neutrino oscillation probabilities through our nonturbulent profiles already experience multiple resonances which lead to phase effects and, these too, drive the probabilities averaged over energy and/or time bins to one half. Thus turbulence is only a difference of degree rather than of kind from the phase effects already present in our results as long as the turbulence affects the neutrinos during the period when they experienced phase effects.

We can investigate this quantitatively by comparing calculations of neutrino propagation through a profile

with and without turbulence by adopting the approach of Fogli *et al.* [51]. Fluctuations are added to the one dimensional density profile at 4.5 s by multiplying the potential, $V_e(r)$, by a factor $1 + F(r)$. The function $F(r)$ is assumed to be a Gaussian field restricted to the region between the forward shock at r_s and the reverse shock at r_r . We adopt a Kolmogorov spectrum for the fluctuations with a lower cutoff wavenumber, k_* , equal to $k_* = 2\pi/(r_s - r_r)$. We represent $F(r)$ by a Fourier series with 1000 modes and use the condition that $F(r)$ vanishes at the two shocks. Thus $F(r)$ is given by

$$F(r) = \sqrt{C} \sum_{n=1}^{1000} A_n \sin[n k_* (r - r_r)] \quad (11)$$

where the A_n are independent random Gaussian variates with variance $\sigma_n^2 = n^{-5/3}$. The constant C sets the scale for the fluctuations and we select C to give an expected rms integrated power in the fluctuations of 15%. This satisfies the limit for strong turbulence in the large θ_{13} case [52]. The density profile with one realization of $F(r)$ is shown in Figure 8 and in Figure 9 we compare the antineutrino survival probabilities as a function of energy for the same two profiles. We see that turbulence causes an expansion of the neutrino energies experiencing phases effects because the noise extends the density range reached between the shocks and thus those neutrinos with resonance densities above and below the range with the nonturbulent profile can now be affected. Upon closer inspection we also find that the phase effects oscillate with energy more frequently. But despite these quantitative differences between the two calculations the overall picture is the same for the two cases leading us to confirm our expectations.

IV. CONCLUSIONS

By performing collective and dynamical numerical calculations of relic supernova neutrino fluxes we have found that the shock effects are considerable if θ_{13} is larger than the threshold of $\sin^2 2\theta_{13} \gtrsim 10^{-5}$. These effects are twofold. First the shocks reduce the sensitivity to the oscillation parameters (θ_{13} in particular). Second there is a loss of sensitivity to the collective effects for the inverse hierarchy and large θ_{13} . This loss of sensitivity to the collective effects and θ_{13} appears to be robust against variations of the neutrino emission, of the details of the density profiles and also against turbulence. We have also shown that the use of analytical formulae without the shock effects can significantly overestimate (or underestimate) the rates. In summary, shock wave effects introduce important modifications of the relic neutrino fluxes and rates and need to be considered in future mod-

elling and simulations¹. To assist further efforts to this end we have proposed a simplified procedure to quantitatively capture the relevant shock wave effects, both in

the relic neutrino fluxes and the associated event rates in observatories on Earth.

-
- [1] J. T. Pantaleone, Phys. Lett. B **287**, 128 (1992).
 - [2] S. Samuel, Phys. Rev. D **48**, 1462 (1993).
 - [3] H. Duan, G. M. Fuller, J. Carlson and Y. Z. Qian, Phys. Rev. D **74**, 105014 (2006) [arXiv:astro-ph/0606616].
 - [4] S. Hannestad, G. G. Raffelt, G. Sigl and Y. Y. Y. Wong, Phys. Rev. D **74**, 105010 (2006) [Erratum-ibid. D **76**, 029901 (2007)] [arXiv:astro-ph/0608695].
 - [5] A. B. Balantekin and Y. Pehlivan, J. Phys. G **34** (2007) 47 [arXiv:astro-ph/0607527].
 - [6] G. G. Raffelt and A. Y. Smirnov, Phys. Rev. D **76**, 125008 (2007) [arXiv:0709.4641 [hep-ph]].
 - [7] B. Dasgupta, A. Dighe, G. G. Raffelt and A. Y. Smirnov, Phys. Rev. Lett. **103**, 051105 (2009) [arXiv:0904.3542 [hep-ph]].
 - [8] R. C. Schirato and G. M. Fuller, arXiv:astro-ph/0205390.
 - [9] C. Lunardini and A. Y. Smirnov, JCAP **0306**, 009 (2003) [arXiv:hep-ph/0302033].
 - [10] K. Takahashi, K. Sato, H. E. Dalhed and J. R. Wilson, Astropart. Phys. **20**, 189 (2003) [arXiv:astro-ph/0212195].
 - [11] G. L. Fogli, E. Lisi, D. Montanino and A. Mirizzi, Phys. Rev. D **68**, 033005 (2003) [arXiv:hep-ph/0304056].
 - [12] R. Tomas, M. Kachelriess, G. Raffelt, A. Dighe, H. T. Janka and L. Scheck, JCAP **0409**, 015 (2004) [arXiv:astro-ph/0407132].
 - [13] G. L. Fogli, E. Lisi, A. Mirizzi and D. Montanino, JCAP **0504**, 002 (2005) [arXiv:hep-ph/0412046].
 - [14] S. Choubey, N. P. Harries and G. G. Ross, Phys. Rev. D **74**, 053010 (2006) [arXiv:hep-ph/0605255].
 - [15] B. Dasgupta and A. Dighe, Phys. Rev. D **75**, 093002 (2007) [arXiv:hep-ph/0510219].
 - [16] S. Choubey, N. P. Harries and G. G. Ross, Phys. Rev. D **76**, 073013 (2007) [arXiv:hep-ph/0703092].
 - [17] J. P. Kneller, G. C. McLaughlin and J. Brockman, Phys. Rev. D **77**, 045023 (2008) [arXiv:0705.3835 [astro-ph]].
 - [18] J. P. Kneller and G. C. McLaughlin, Phys. Rev. D **73**, 056003 (2006) [arXiv:hep-ph/0509356].
 - [19] J. Gava, J. Kneller, C. Volpe and G. C. McLaughlin, Phys. Rev. Lett. **103**, 071101 (2009) [arXiv:0902.0317 [hep-ph]].
 - [20] L. M. Krauss, S. L. Glashow and D. N. Schramm, Nature **310** (1984) 191.
 - [21] A. Dar, Phys. Rev. Lett. **55** (1985) 1422.
 - [22] T. Totani, K. Sato and Y. Yoshii, Astrophys. J. **460** (1996) 303 [arXiv:astro-ph/9509130].
 - [23] R. A. Malaney, Astropart. Phys. **7** (1997) 125 [arXiv:astro-ph/9612012].
 - [24] M. Kaplinghat, G. Steigman and T. P. Walker, Phys. Rev. D **62** (2000) 043001 [arXiv:astro-ph/9912391].
 - [25] M. Fukugita and M. Kawasaki, Mon. Not. Roy. Astron. Soc. **340** (2003) L7 [arXiv:astro-ph/0204376].
 - [26] S. Ando and K. Sato, New J. Phys. **6**, 170 (2004) [arXiv:astro-ph/0410061].
 - [27] C. Lunardini, Astropart. Phys. **26**, 190 (2006) [arXiv:astro-ph/0509233].
 - [28] H. Yuksel and J. F. Beacom, Phys. Rev. D **76**, 083007 (2007) [arXiv:astro-ph/0702613].
 - [29] M. Aglietta *et al.*, Astropart. Phys. **1**, 1 (1992).
 - [30] M. Malek *et al.* [Super-Kamiokande Collaboration], Phys. Rev. Lett. **90** (2003) 061101 [arXiv:hep-ex/0209028].
 - [31] D. Autiero *et al.*, JCAP **0711**, 011 (2007) [arXiv:0705.0116 [hep-ph]].
 - [32] A. G. Cocco, A. Ereditato, G. Fiorillo, G. Mangano and V. Pettorino, JCAP **0412**, 002 (2004) [arXiv:hep-ph/0408031].
 - [33] C. Volpe and J. Welzel, arXiv:0711.3237 [astro-ph].
 - [34] J. F. Beacom and M. R. Vagins, Phys. Rev. Lett. **93**, 171101 (2004) [arXiv:hep-ph/0309300].
 - [35] L. E. Strigari, J. F. Beacom, T. P. Walker and P. Zhang, JCAP **0504** (2005) 017 [arXiv:astro-ph/0502150].
 - [36] H. Yuksel, M. D. Kistler, J. F. Beacom and A. M. Hopkins, Astrophys. J. **683**, L5 (2008) [arXiv:0804.4008 [astro-ph]].
 - [37] S. Chakraborty, S. Choubey, B. Dasgupta and K. Kar, JCAP **0809**, 013 (2008) [arXiv:0805.3131 [hep-ph]].
 - [38] W. C. Haxton and C. W. Johnson, Nature **333**, 325 (1988).
 - [39] R. Lazauskas, C. Lunardini and C. Volpe, JCAP **0904**, 029 (2009) [arXiv:0901.0581 [astro-ph.SR]].
 - [40] F. J. Botella, C. S. Lim and W. J. Marciano, Phys. Rev. D **35** (1987) 896.
 - [41] J. Gava and C. C. Jean-Louis, arXiv:0907.3947 [hep-ph].
 - [42] J. Gava and C. Volpe, Phys. Rev. D **78**, 083007 (2008) [arXiv:0807.3418 [astro-ph]].
 - [43] A. Arcones, H. T. Janka and L. Scheck, arXiv:astro-ph/0612582.
 - [44] I. K. Baldry and K. Glazebrook, Astrophys. J. **593**, 258 (2003) [arXiv:astro-ph/0304423].
 - [45] C. Amsler *et al.* [Particle Data Group], Phys. Lett. B **667**, 1 (2008).
 - [46] A. B. Balantekin, J. Gava and C. Volpe, Phys. Lett. B **662**, 396 (2008) [arXiv:0710.3112 [astro-ph]].
 - [47] J. P. Kneller and G. C. McLaughlin, Phys. Rev. D **80**, 053002 (2009) [arXiv:0904.3823 [hep-ph]].
 - [48] A. S. Dighe and A. Y. Smirnov, Phys. Rev. D **62**, 033007 (2000) [arXiv:hep-ph/9907423].
 - [49] S. Ando and K. Sato, Phys. Lett. B **559**, 113 (2003) [arXiv:astro-ph/0210502].
 - [50] C. Lunardini, B. Muller and H. T. Janka, Phys. Rev. D **78**, 023016 (2008) [arXiv:0712.3000 [astro-ph]].
 - [51] G. L. Fogli, E. Lisi, A. Mirizzi and D. Montanino, JCAP **0606**, 012 (2006) [arXiv:hep-ph/0603033].
 - [52] A. Friedland and A. Gruzinov, arXiv:astro-ph/0607244.
 - [53] H. Duan and J. P. Kneller, J. Phys. G **36**, 113201 (2009) [arXiv:0904.0974 [astro-ph.HE]].
 - [54] B. Dasgupta and A. Dighe, Phys. Rev. D **77**, 113002 (2008) [arXiv:0712.3798 [hep-ph]].